Available online at www.sciencedirect.com
SCIENCE DIRECT®
Polymer 44 (2003) 6537–6547
polymer
www.elsevier.com/locate/polymer

Plastic damage mechanisms of polypropylene/polyamide 6/polyethelene-octene elastomer blends under cyclic tension

Shu-Lin Bai*, Min Wang

Department of Mechanics and Engineering Science, Peking University, 100871 Beijing, People's Republic of China

Received 29 May 2003; received in revised form 6 August 2003; accepted 7 August 2003

Abstract

A series of three-phase polymer blends, composed of polypropylene (PP) matrix, polyamide-6 (PA6) fillers and polyethylene-octene elastomer grafted with maleic anhydride (POE-*g*-MA) modifiers, were designed and manufactured. Their mechanical behavior under cyclic loading–unloading was studied by using a video-controlled testing system named as VideoTraction© system. It was found that with the increasing PA6 and POE content, the strain hardening became more and more prominent, the volume strain decreased, and the energy dissipated increased. A detailed examination of the cryo-fractured surfaces under SEM was undertaken. The microcavity nucleation, growth and coalescence were observed, and represent the main mechanisms of plastic deformation and damage. The high volume strain comes from the abundant formation of microvoids. On the contrary, the formation of microvoids resulted in relatively smaller quantity of energy dissipation. This result coincides well with the toughening mechanisms of polymer blends revealed by other peoples.

Keywords: Ternary polymer blends; Plastic damage; Volume strain

1. Introduction

The ternary polymer blends consisted of polypropylene (PP), polyamide (PA6 or PA66) and elastomer have been studied widely in the world in the past half century. These works aimed initially to improve the compatibility between polypropylene and polyamide, and then to establish the relationship between the morphology and mechanical behavior of such ternary polymer blends. The blend systems studied, up till now, include PP/PA66/SEBS-*g*-MA [1–5], PP/PA6/EPR-*g*-MA [3–5], PP/PA6/PP-*g*-MA [6], PP/PA6/EPDM-*g*-MA [7], etc. Two years ago, a research group has initiated a research project on polypropylene, polyamide 6 and polyethylene-octene elastomer (POE) blends, some results were already published [8–9].

It is well known that neat polypropylene is incompatible with neat polyamide. In order to improve the compatibility between them, a third constituent needs to be added. The maleated polypropylene was proved to be effective to do this. The rigidity and strength of such modified blends were increased, but the impact toughness was decreased due to the strong adhesion across the interface. Therefore, other attempts concentrated mainly on how to increase the impact toughness by adding an elastomer element into the blends. The elastomer phase added, either independently dispersed in the matrix in the form of spherical phase, or encapsulating the dispersed PA or PP phase forming core-shell structures, could bring a significant increase of impact strength. The morphology of such blends with three constituents is much complicated and depends on the proportion of the constituents. The continuous matrix phase in general is the constituent with maximum content, and other two disperse randomly in the matrix in form of isolated spheres or ellipsoids. When the proportion of the two maximum content constituents is close or same to each other, the dispersed phase may have an irregular shape and even contain sometimes small matrix phase inside it. The study on the mechanical behavior of PP/PA/elastomer blends was conducted principally by putting the emphasis on the reinforcing and toughening effect. Tensile, impact tests as well as dynamic tests (DMTA) were often performed.

A domain that is not, until now, explored widely and deeply is the plastic deformation and corresponding damage mechanisms. Early works on the necking phenomenon in

* Corresponding author. Tel. +86-10-63-75-14-44; fax: +86-10-62-75-14-44.
E-mail address: slbai@pku.edu.cn (S.L. Bai).

0032-3861/$ - see front matter © 2003 Elsevier Ltd. All rights reserved.
doi:10.1016/S0032-3861(03)00739-0

tensile tests were extensively documented in the literature [10]. The plastic deformation can be produced by two mechanisms: shear banding and cavitation. The latter can result in a volume expansion of the samples deformed. Therefore, volume change is considered to be a phenomenon accompanied with the plastic deformation and damage in polymer blends. Bucknall et al. [11] studied the dilatation of HIPS under creep tests by measuring the dilatation with a special extensometer. They found that crazing is an important form of damage in brittle matrix blends. Cavitation was identified as an active mechanism for rubber toughened polymers. Gent et al. [12] revealed the process of cavity formation for a rigid inclusion filled elastomer under uni-axial tension. G'Sell et al. [13] working on a rubber toughened PMMA showed that large damage rate was attributed to the formation and growth of voids in the rubber shell of the toughening particles. The decohesion at glass bead/HDPE interface was observed and the decohesion stress decreased with the decreasing bonding strength at the interface [14]. Meddad and Fisa [15] showed that glass bead/PP system underwent a high damage rate, due to the decohesion of the beads. Pukanszky et al. [16] studied the $CaCO_3$ filled polypropylene composites. They found that the dominating deformation process was debonding at PP/$CaCO_3$ interface, and the initiation stress for void formation was close to yield stress. The interfacial debonding was also observed for PP/PA6/POE-*g*-MA blends in our previous investigation [8].

Many investigations on the plastic damage of polymer blends were fulfilled under the conditions of monotonic and impact loading. The information obtained represents the final state of plastic deformation. Unfortunately, the deformation process and corresponding microstructural evolution are unknown. The accumulation of plastic damage under cyclic or fatigue loading is seldom studied. Recently, Meyer and Pruitt [17] studied the cyclic loading effect on the morphology, structure and relaxation of ultra high molecular weight polyethylene. The crazing, microvoid formation and lamellae alignment were found to vary with increasing amount of true strain and number of cycles. Bai et al. [18] found that for glass beads filled HDPE, the damage under cyclic loading–unloading tests could be expressed by the change of elastic modulus. The residual strain after each loading–unloading cycle increased with increasing applied strain. A model to the elastoplastic response under loading–unloading tests was proposed by Drozdov and Christiansen [19]. Isotactic polypropylene was used as a target material. A linear growth of the rate of plastic strain with the maximum plastic strain was found, which was caused by the coarse slip and fragmentation of lamellae at unloading.

In this paper, the plastic damage behavior of PP/PA6/-POE-*g*-MA blends under cyclic tension is investigated. The true stress–strain, volume variation and energy dissipation are measured. The plastic damage mechanisms are revealed with SEM. The results obtained are original and helpful to well understand the mechanical behavior of polymer blends under large deformation.

2. Materials and experimental methods

2.1. Materials

The compositions of the blends studied in this work are listed in Table 1. The polypropylene (PP401) was obtained from Liaoyang Petrochemical Corp., P.R. China. Shanghai Plastics Production Factory No. 18, P.R. China, supplied the polyamide-6 (PA6). The polyethylene-octene elastomer (POE) with octene content of 9.5% and melt flow index of 3.5 g/10 min was obtained from Dow Chemical Co. POE-*g*-MA was synthesized in laboratory and its grafting ratio is about 1% in weight.

All materials were dry blended together in a high-speed blender following the pre-designed composition ratios. Then a co-rotating Φ30 mm twin-screw extruder (SHJ-30) was employed at a screw speed of 110 rpm and barrel temperatures of 190–200–210–200 °C. The pelletized blends were dried and injection molded into standard ASTM specimens in an injection-molding machine (SZ-160/80 NB) for mechanical tests.

2.2. Video-controlled tensile tests

In order to localize the deformation in the region where all mechanical variables are determined, a geometric defect was machined in the centre of ASTM D638M standard specimens. The defect, which extends over a length of 10 mm, corresponds to a reduction of width with a rounded profile. Consequently, the minimum cross-section was a rectangle of 8×4 mm^2.

The measurements of the strain were accomplished with the help of seven markers printed on the sample surfaces as shown in Fig. 1. The markers are white, nearly round, with a diameter of about 0.4 mm. The five markers (A, B, C, D, E) aligned along the tensile axis x_3, with the inter-distance of markers of 1 mm. The three markers (F, C, G) aligned along the transverse axis x_1, are more widely separated, in such a way that they occupy a major fraction of the total width in the geometric defect. A representative volume element having a thickness of 0.2 mm is taken as the element on which the transverse strain and applied stress are measured.

Table 1
Composition and proportion of the blends studied

Blends	PP (wt%)	PA6 (wt%)	POE-*g*-MA (wt%)
PP	100	–	–
BD13	85	10	5
BD14	70	20	10
BD15	55	30	15
BD16	40	40	20

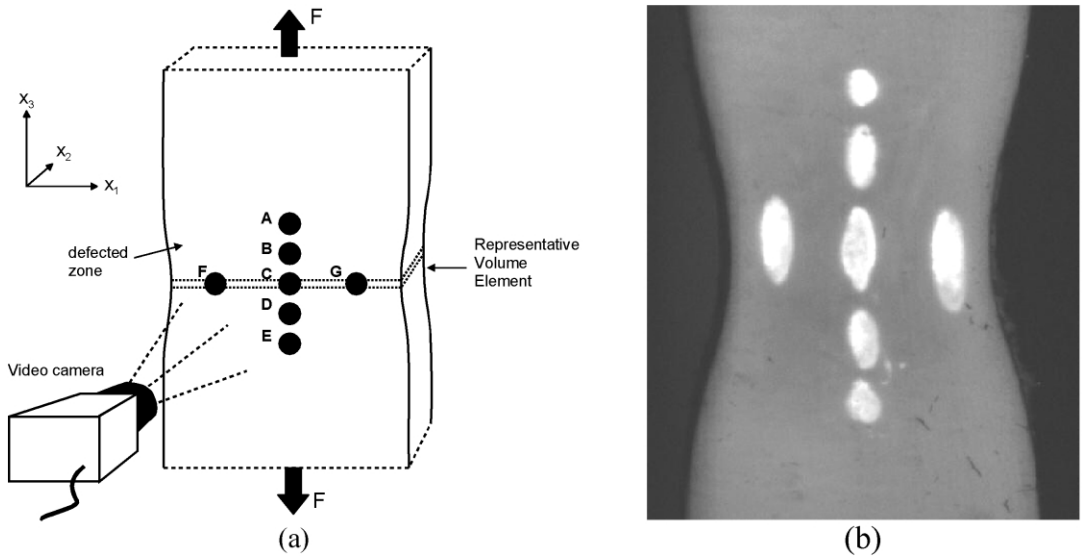

Fig. 1. Configuration of the 7 markers in the video-controlled tensile testing system, (a) schematic diagram [20], (b) micrograph of a sample deformed.

The diagram in Fig. 2 shows the main feature of the VideoTraction© system. The details on the strain calculation can be found in the publication by G'Sell [20]. Such samples are stretched by the way of cyclic loading–unloading on a MTS810, under constant strain rate of 1.1×10^{-3}/s.

In order to reveal the mechanisms of plastic damage, a series of monotonically tensile tests were undertaken with a small universal testing stage, which has the maximum load of 2 kN. To control the strain magnitude applied, the white spots were painted on the surface of non-standard samples just as in the case of cyclic tests. The loading was interrupted when the true strain reached a given value, which varied from 0.2 to 1.2 with the increment of 0.2. The samples deformed were then cryo-fractured. The cryo-fractured surfaces were coated with a layer of gold and then observed under a scanning electron microscope (KYKY-960). Fig. 3 shows the schematic process of sample preparation for SEM observation.

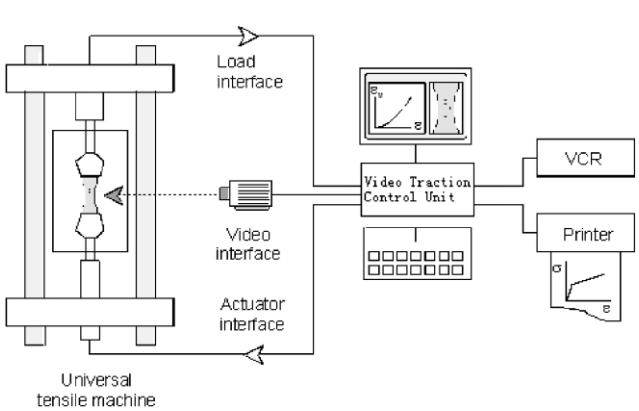

Fig. 2. General diagram of the VideoTraction© system [20].

3. Results and discussion

3.1. True axial stress vs. strain behavior under cyclic tension

The cyclic tensile curves of studied materials are shown in Fig. 4. A progressive decrease of yield stress with alloying content is remarked. The strain softening phenomenon became less important with increasing alloying content, even disappeared for the blends of BD15 and BD16 with high PA6 and POE content (PA6 = 30, 40 wt% and POE = 15, 20 wt%). In reality, the strain hardening of BD16 has taken place immediately after the yielding without the occurrence of strain softening. It is know that the strain softening of a material is often caused by the nucleation and growth of microvoids inside the materials. On the contrary, the strain hardening is produced by massive shear banding of the matrix. This means that the mechanisms of plastic deformation for BD13 and BD14 differ from that of BD15 and BD16. The true stress–strain curve of neat PP situates between that of BD13 and BD14, and that of BD15 and BD16. It seems that the deformation mechanisms of neat PP are probably controlled by both microvoids formation and matrix shear banding. A discussion on this is given later in Section 3.4. The hysteresis loops are similar in shape for all materials. The viscous characteristics of the blends are manifested by the non-linearity of unloading curves.

After each unloading to zero load, the strain did not return to zero. The residual strain just after unloading depends on the level of applied strain as shown in Fig. 5. The difference of residual strain among the blends is small. The residual strain will diminish with the time as revealed by Meyer [17]. In our case, the time effect is not studied. But, from the different curves under tension (Fig. 4), we

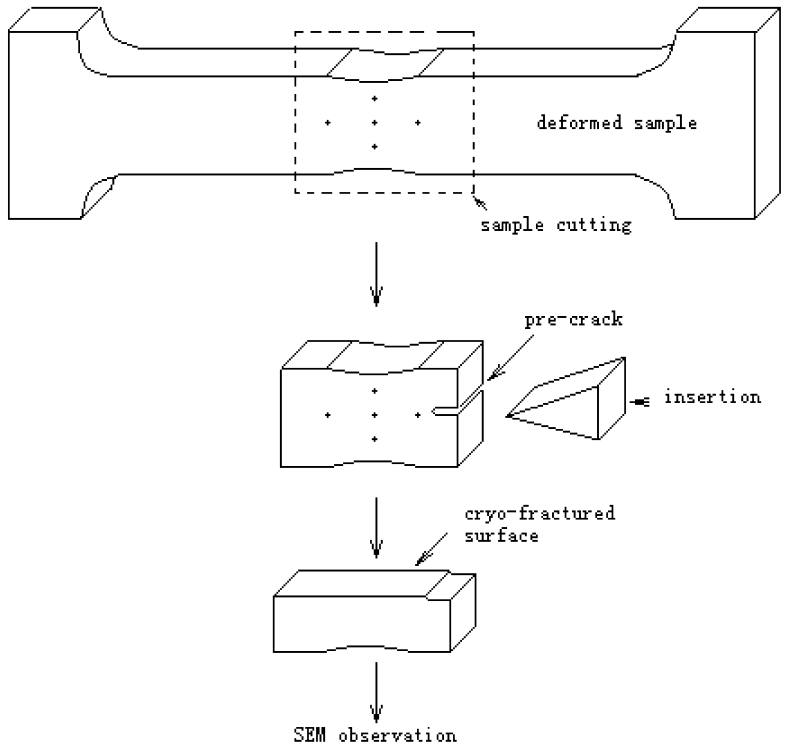

Fig. 3. Schematic presentation of sample taking off for SEM observation.

believe that the relaxation behavior presented by residual strain vs. time will be different for the blends studied.

3.2. Volume strain

The volume strain is defined as $\varepsilon_v = \varepsilon_1 + \varepsilon_2 + \varepsilon_3$, where ε_i ($i = 1, 2, 3$) represents true strain in three directions as shown by x_1, x_2 and x_3 in Fig. 1. In our case, the load was applied along x_3 direction. ε_1 and ε_3 were measured with the VideoTraction system. As to ε_2, an approximate assumption is made as $\varepsilon_1 \approx \varepsilon_2$, therefore $\varepsilon_v \approx 2\varepsilon_1 + \varepsilon_3$. This assumption was initially adopted by G'Sell [13]. This equality between ε_1 and ε_2 is valid only when two following conditions are met. First one is that the material is isotropic or transversely isotropic around the loading axis (x_3). Second is that the sample width is not much greater than its thickness in order to maintain plan-strain tension, which gives the uniform deformation of the samples through thickness. First condition is satisfied automatically since BD13 and BD14 are isotropic, and BD15, BD16 can be considered to be transversely isotropic with long axis of ellipsoidal PA6 phases lying along the loading direction. The sample width is twice that of its thickness (8 mm against 4 mm). This sample geometry can result in, in our opinion, an approximate uniform deformation along x_1 and x_2 directions. In fact, ε_2 can vary from 0 to ε_1, corresponding to very thin (thickness is far less than width) and very thick (thickness is equal to width) samples,

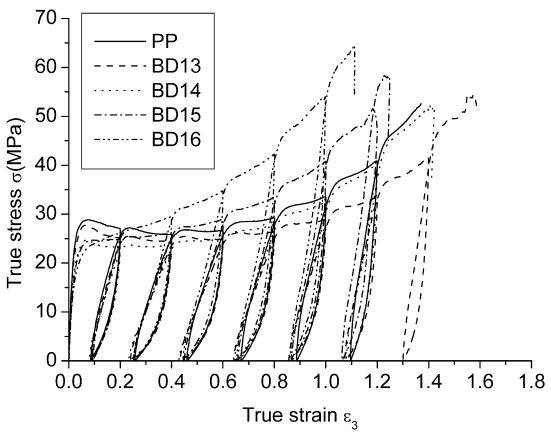

Fig. 4. True stress–strain relationship under cyclic tension.

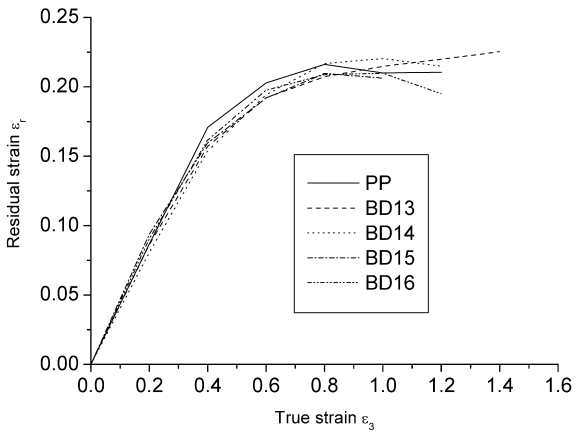

Fig. 5. Residual strain vs. applied true strain for each cycle.

respectively. If taking the average value $\varepsilon_2 = 0.5\varepsilon_1$, the results of volume strain may be more reasonable. Anyway, the experimental confirmation must be given, not here, but in the future work.

The volume strain versus axial true strain curves are shown in Fig. 6 for all blends and neat polypropylene. On the whole, the volume strain increased almost linearly in the first stage corresponding to elastic deformation, and then progressively with the applied true strain. A saturation of volume strain seems to appear when axial true strain reached a large value. The saturation strain, i.e. applied true strain at the saturation moment of volume strain decreased with the alloying content, from about 1.3 for BD13 to 0.8 for BD16. If connecting together the saturation points of all materials, a straight line can be drawn as shown in Fig. 6. It is noted that, at a given axial true strain, the volume strain decreased with the alloying content. The volume strain of neat PP has the same trend of variation as that of the blends, but dropped among the values for the blends when the applied strain is great. This phenomenon corresponds well to the tensile curves in Fig. 4. The volume strain diminished as the unloading was applied. The quantity of reduced volume strain increased with the cycle or applied true strain, and decreased with the increasing alloying content. This remark is interesting and worthy to study further in that even though the load was returned to zero, the residual volume strain was still great.

3.3. Energy dissipated

Fig. 7 is schematically given the definition of energy dissipation during each loading and unloading cycle. Here, the term of 'energy' means the energy density, i.e. energy per unite of volume. The whole energy is composed of elastic energy E_e, represented by the area of shadow region, and plastic energy E_p, by the area of white region. The elastic energy is released after unloading to zero load. The plastic energy is further divided into two parts: one from matrix shear banding and another from the cavitation. From the experimental results, it is impossible to separate these two parts of plastic energy.

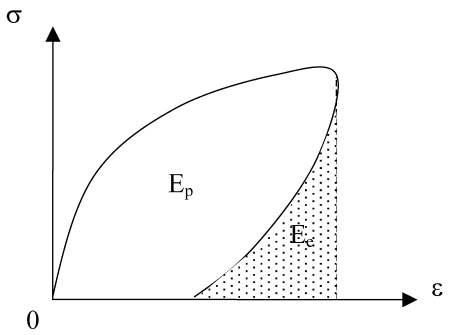

Fig. 7. Definition of energy dissipated (E_p) and elastic one (E_e).

During the process of loading, the temperature of samples can rise up due to the following reasons: elastic deformation, plastic deformation and internal heat supply in general. In our case, no internal heat was supplied. The heat created by the elastic and plastic deformation contributes, in one part, to the temperature rising of the samples and diffuses by heat exchange with the environment in another part. In the case of adiabatic deformation such as dynamic test, no heat exchange with the environment happens. In this work, the strain rate is 1.1×10^{-3}/s, the heat exchange has surely taken place and is not included unfortunately in the total energy calculation. We need to do further test to measure it directly. However, we consider that this energy by heat diffusion takes a small part in the total energy. Most of the energy was consumed by the elastic and plastic deformation including the influence of temperature rising, which was calculated and shown in Figs. 8 and 9.

The curves in Fig. 8 represent the whole energy dissipated during the loading–unloading cycles. At early stage of deformation with true strain below 0.4, the total energy absorbed is not much different for the materials studied. However, with the increasing true strain, the increase of total energy for neat PP, BD13 and BD14 with low alloying content became slower compared to BD15 and

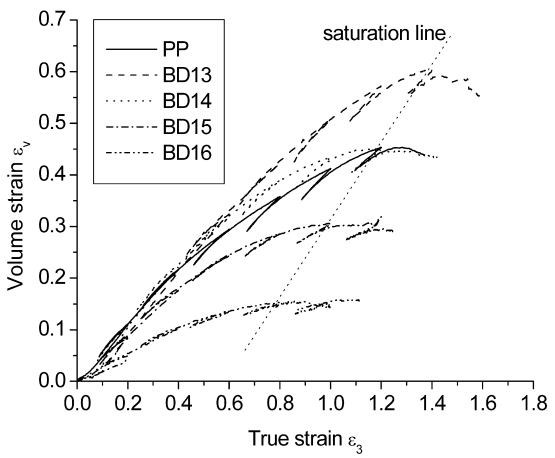

Fig. 6. Volume strain vs. true strain under cyclic tension.

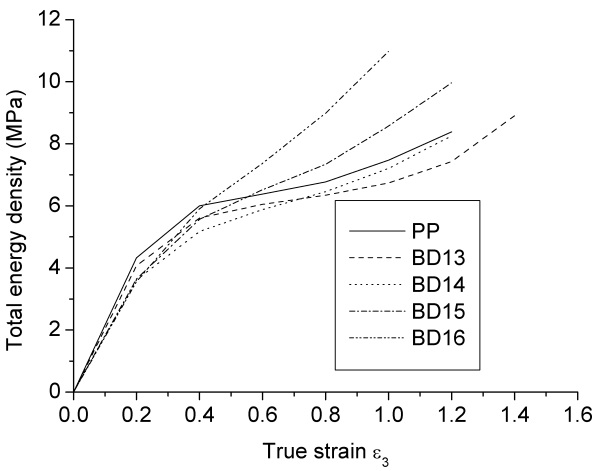

Fig. 8. Total energy density vs. applied true strain for cyclic tension.

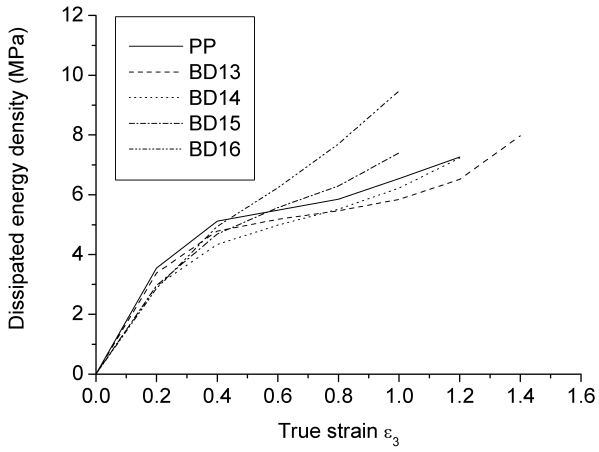

Fig. 9. Energy dissipated vs. applied true strain for cyclic tension.

BD16 with high alloying content. The aberration of the curves between the blends with low and high alloying content is larger and larger as the true strain continues to increase. This attendance of variation signifies also that only when the deformation reaches a certain level, the contribution of different deformation mechanisms to the energy dissipation can be clearly identified.

By removing the elastic energy (which takes about 10–20% of total energy), the plastic energy vs. the true strain is shown in Fig. 9. These curves in Fig. 9 are similar in shape to those in Fig. 8. This means that the elastic energy for all materials is not much different. From the results shown in Figs. 8 and 9, the energy dissipation for neat PP is always moderate, compared with the blends.

Now, let us to discuss the relationship between the volume strain and energy dissipated, based on the curves presented in Figs. 6 and 9. It is noted that the large volume strain corresponds to small energy dissipation such as in the case of BD13 and BD14. Large volume strain comes from the abundant nucleation and growth of cavities inside the samples. The small energy value with large volume strain means that the cavitation is not the main source for energy dissipation. Polymer scientists accept the point of view that, for polymer blends and particle filled polymers, the energy dissipation comes mainly from the matrix shear deformation, instead of cavitation. It is stated previously that shear deformation cannot result in volume change. Therefore, we have the reason to conclude that for the blends of BD15 and BD16 with high alloying content, matrix shear deformation is the controlling factor for energy dissipation, without causing large volume change.

Except for yield stress and Young's modulus, other properties such as volume strain, true stress–strain curves and dissipated energy for neat PP fall between the two blends with high alloying content and the two blends with low alloying content. By taking a close examination, it was found that this phenomenon appeared only after the yielding, i.e. the true strain reached 0.2 for true stress–strain and volume strain, and 0.4 for dissipated energy. In this stage, deformation is strongly influenced by the damage development. For neat PP, the damage was created by the crack nucleation between the lamellars of spherulite crystals, which was proved by our SEM observation for monotonic loading and will be published later. The damage develops by the crack growing and new crack nucleation.

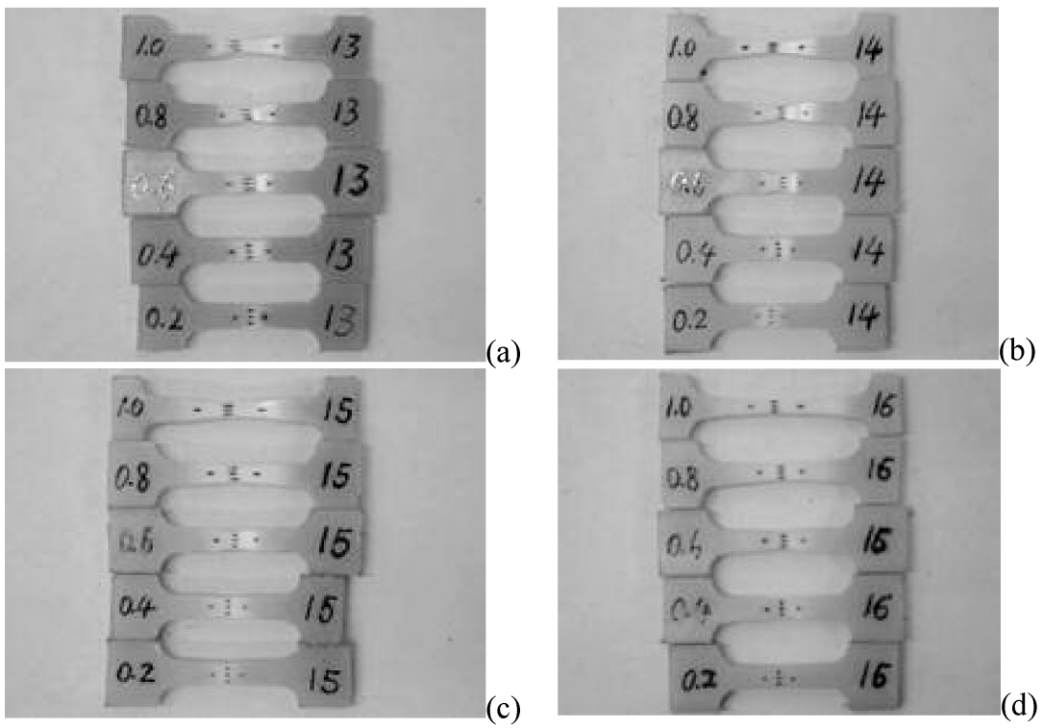

Fig. 10. In situ test samples deformed under different true strain; (a) BD13, (b) BD14, (c) BD15, (d) BD16.

The damage mechanisms for the blends are different from that of PP. According to the micrographs presented in Figs. 11–14 and the statements cited in the corresponding paragraph, the damage evolution for the blends is a process of microvoids nucleation, growing and coalescence at the two poles of particles. Owing to the difference of the quantity and size of dispersed PA6 particles among the blends, the response to the external load is different, reflected by the stress–strain relation, volume strain and energy dissipation. It is considered that the damage development of neat PP may be moderate compared to the blends. That's the reason why neat PP falls always between the blends with high alloying content and that with low alloying content. A quantitative description of the damage degree and the difference among the materials should be made by measuring the density of microcracks and cavity, which is a heavy task to be completed in the future.

According to the DSC measurement, the crystallinity of neat PP is about 0.51. The crystallinity of PP in the blends changed from 0.64 for BD13 to 0.59 for BD16. This increase of crystallinity could have an influence on the mechanical behavior of the blends. But, the deformation behavior after the yielding or under large deformation is mainly controlled by the damage development.

3.4. Mechanisms of plastic deformation and damage

Above analysis on the deformation mechanisms is deduced from the tensile curves without solid proofs. Now, in situ tensile tests aimed to reveal the real mechanisms of plastic deformation and damage were carried out with a small tensile stage. The pictures taken after each test from the deformed samples are gathered together in Fig. 10. Each sample underwent a given true strain magnitude from 0.2 to 1.0, they are greater than the yield strain of about 0.05 for all blends. The figures written on the left end of each sample represent the final true strain values applied to the sample, while the figures on the right are the number of material serial. The color of the samples is brighter with the increasing PA6 or POE content. From the appearance of the samples deformed, two features are noted. Firstly, the greater the PA6 or POE content is, the smaller the extension or necking of the samples. Secondly, the whitening phenomenon is more outstanding for the blends with less alloying elements (BD13 and BD14) than that with

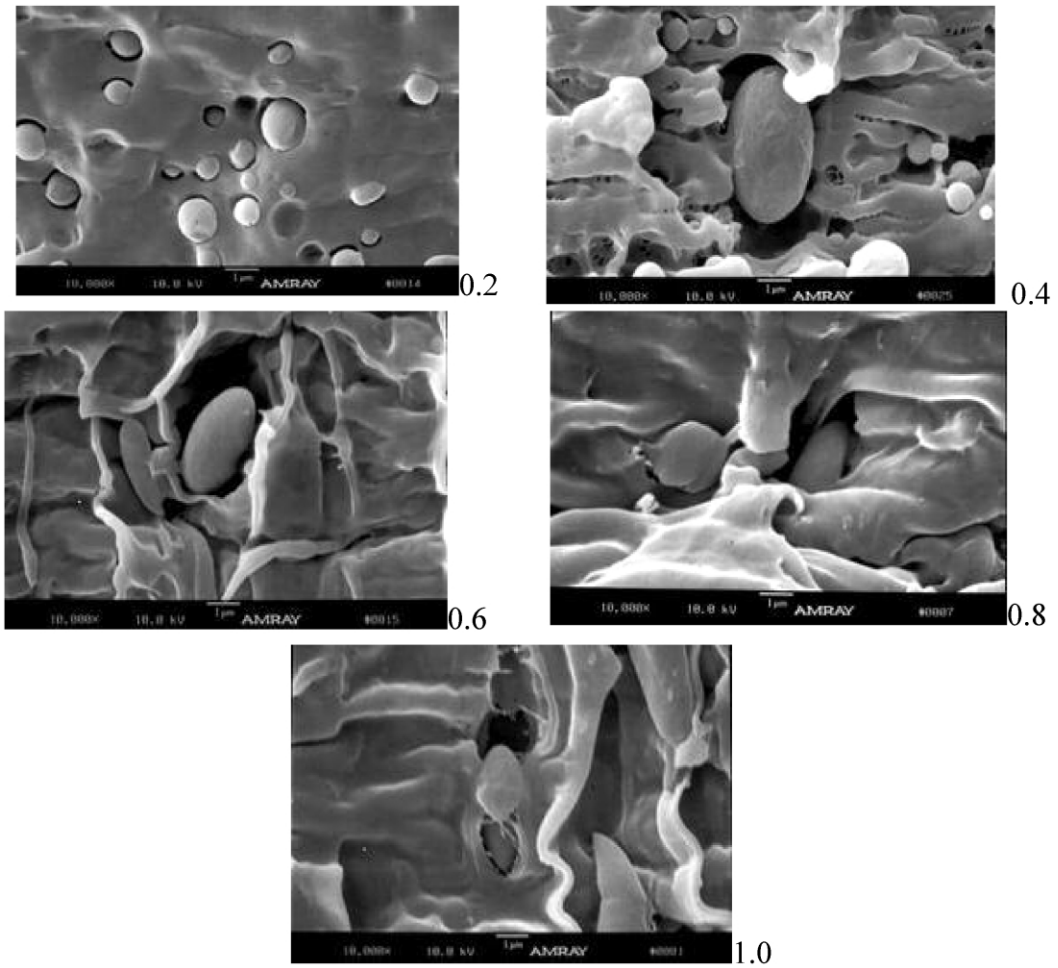

Fig. 11. Cryo-fractured surfaces of BD13 (figures on the micrograph indicating the level of applied true strain). Vertical loading.

more alloying elements (BD15 and BD16). The whitening is generally produced by the crazes and cavities created during the loading. This observation gives the information on the deformation and damage mechanisms and provides the proofs to the analysis made in the previous section. It should be indicated that the samples for in situ tension are not standard, so the geometry and size of the samples are not identical exactly.

The microstructural characteristics of plastic deformation and damage are analyzed with the help of micrographs on the cryo-fractured surfaces taken from the samples deformed and along the loading direction, as presented schematically in Fig. 3. Detailed analysis is stated below.

3.4.1. Blend BD13 (Fig. 11)

At 0.2 true strain, the matrix deformation is small, which is proved by the even and smooth cryo-fractured surfaces. However, the interfacial debonding has taken place, especially at the interface of large PA6 particles. The interfacial crack at one pole of the particle has the form of crescent moon. As the applied strain increased further to 0.4, the stress dropped slightly according to the tensile curves. The microstructure manifests two evolutional characteristics: interfacial crack growing and transforming into microvoid, crack propagating horizontally through several PA6 particles. The evolution of the microstructural morphology continued with the strain increasing to 0.6–1.0. The coalescence of the microvoids by the horizontal propagation of interfacial cracks has taken place, as shown by the micrograph at 0.8 true strain. Some large PA6 particles were completely debonded from the matrix. Besides, the matrix ligaments lying in the loading direction were observed on the surface showed by the micrographs at 0.6 and 1.0 true strain. From above observation, the volume increase comes from the microvoids formed at two poles of particles and the cracks formed perpendicular to the loading direction (Fig. 11).

3.4.2. Blend BD14 (Fig. 12)

Compared with BD13, at low strain of 0.2, the matrix appearance is similar, but less particles were debonded from the matrix. At 0.4 true strain, the matrix deformation and microvoid formation are also less important than BD13.

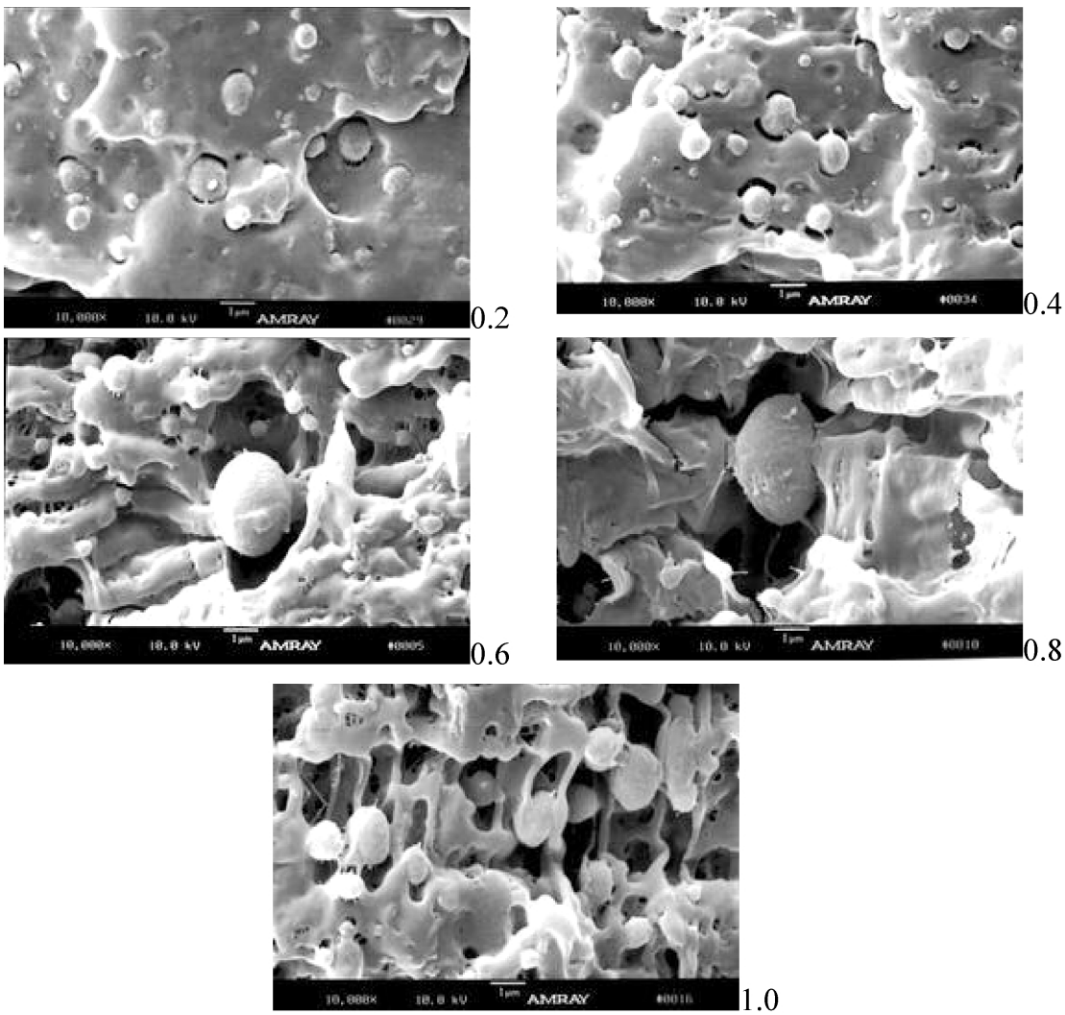

Fig. 12. Cryo-fractured surfaces of BD14 (figures on the micrograph indicating the level of applied true strain). Vertical loading.

Large matrix deformation and large quantity of microvoids were created when the true strain reached 0.6. The microfilaments across the interface can be seen for some small size particles. Even though the microvoid nucleation and growth developed greatly in the region close to the particles, the horizontal cracks are seldom observed. At large true strain of 0.8, the microvoids formed at two poles of PA6 particles grew so greatly that transverse cracks were initiated and propagated. A lot of microvoids were engendered at 1.0 true strain, forming the cavity bands, which contain a large quantity of small PA6 particles. The matrix ligaments between two close PA6 particles were stretched greatly along the loading direction. The main reasons for plastic deformation and damage are same as BD13. But, the volume increase of BD14 is smaller than BD13 (Fig. 12).

3.4.3. Blend BD15 (Fig. 13)

As to BD15, a remarkable character is that the dispersed PA6 particles have the ellipsoidal shape, instead of spherical one as in the case of BD13 and BD14. The long axis of spheroid coincides with the loading direction (also the length direction of molded samples). At average, the size of PA6 spheroid in BD15 is bigger than the spheres in BD13 and BD14. Under low strain magnitude of 0.2, the interfacial debonding appeared for small spherical (existing seldom) and large ellipsoidal PA6 particles. The growth of interfacial cracks with the increasing true strain is not as important as in the case of BD13 and BD14. It seems that not only at the interface, but also in the matrix far from the particles, the cavitation has happened. The cavitation in matrix was probably caused by the dispersed POE phase. No horizontal cracks are created. Interfacial debonding is still the main mechanism of volume expansion. But, the number of dispersed particles is less than that in BD13 and BD14, so the resulted volume strain is smaller. The shearing matrix deformation between two particles is considered to be the principle contribution to the toughening effect (Fig. 13).

3.4.4. Blend BD16 (Fig. 14)

As to BD16, different characters on the morphology of cryo-fractured surfaces are remarked. The interfacial

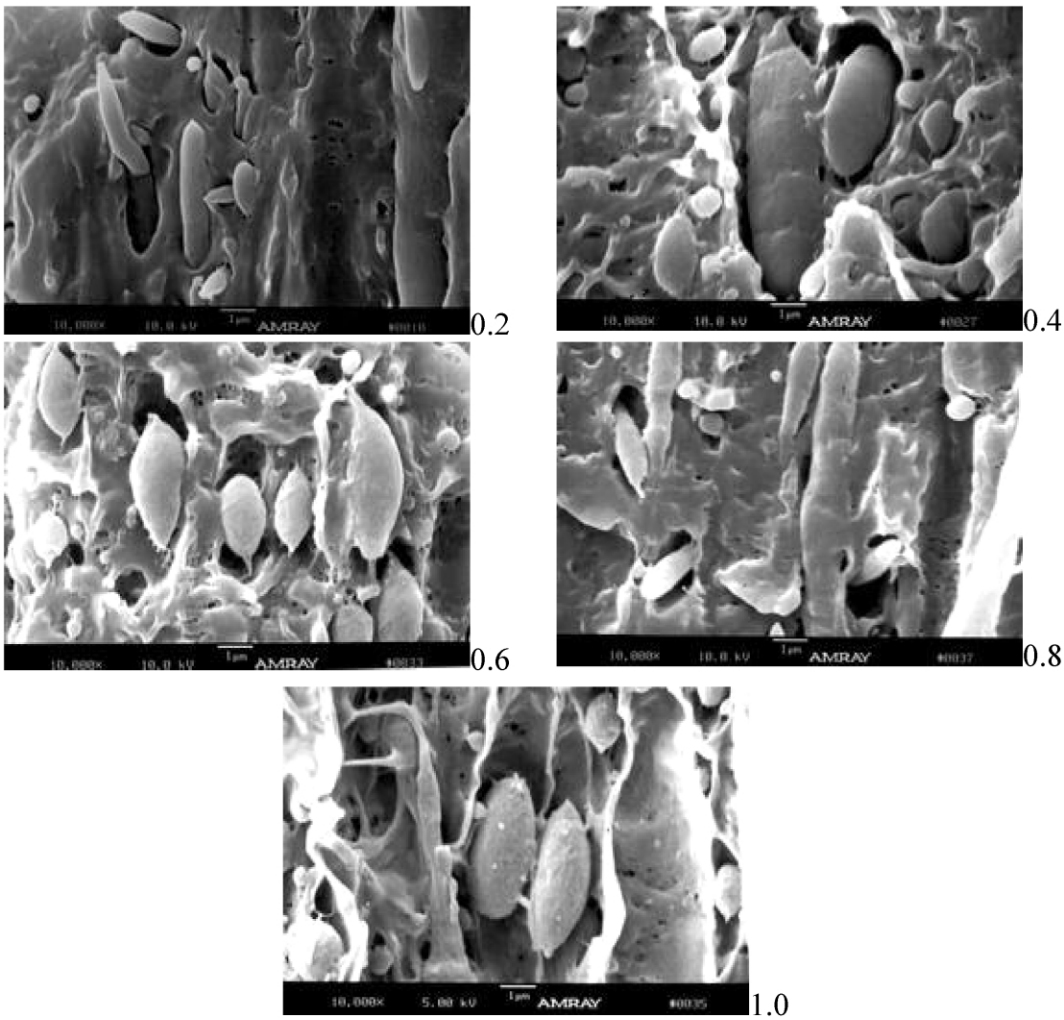

Fig. 13. Cryo-fractured surfaces of BD15 (figures on the micrograph indicating the level of applied true strain). Vertical loading.

debonding can be seen only when the true strain reached certain level (0.4 and 0.6). A certain quantity of microcavities in matrix were created with the increasing true strain. We consider that the dispersed POE phases may be the resources of the cavitation in matrix. At high true strain of 0.8 and 1.0, the interfacial debonding became important and even turned into microcavities by expanding and growing into matrix. However, the number of dispersed PA6 particles is so small that the cavitation at the interface cannot result in great volume increasing. The high toughness of BD16 comes evidently from matrix shearing deformation, as well as the cavitation and deformation of POE phase, which exists probably both at the interface forming core-shell structure and in the matrix (Fig. 14).

4. Conclusions

For ternary polymer blends, their mechanical behavior depends strongly on the proportion of the constituents. In the case of PP/PA6/POE-*g*-MA blends, following conclusions could be reached. On the whole, with the increase of PA6 and POE content,

(1) The yield stress and volume strain decreased, while energy dissipation increased,
(2) The strain softening disappeared and strain hardening became important.

According to detailed examination of the cryo-fractured surfaces under SEM, the volume dilatation was produced by the interfacial debonding at two poles of the particles. The interfacial cracks transformed progressively into microcavities with the increasing applied strain. However, large volume strain corresponds to low energy dissipation. This result proves the basic viewpoint for the toughening mechanisms of polymer blends, i.e. the energy dissipation is caused mainly by the matrix shearing deformation, instead of cavitation, which results in volume change. The relationship between the volume strain and energy dissipation can well explain the damage mechanisms and toughening effect of polymer blends.

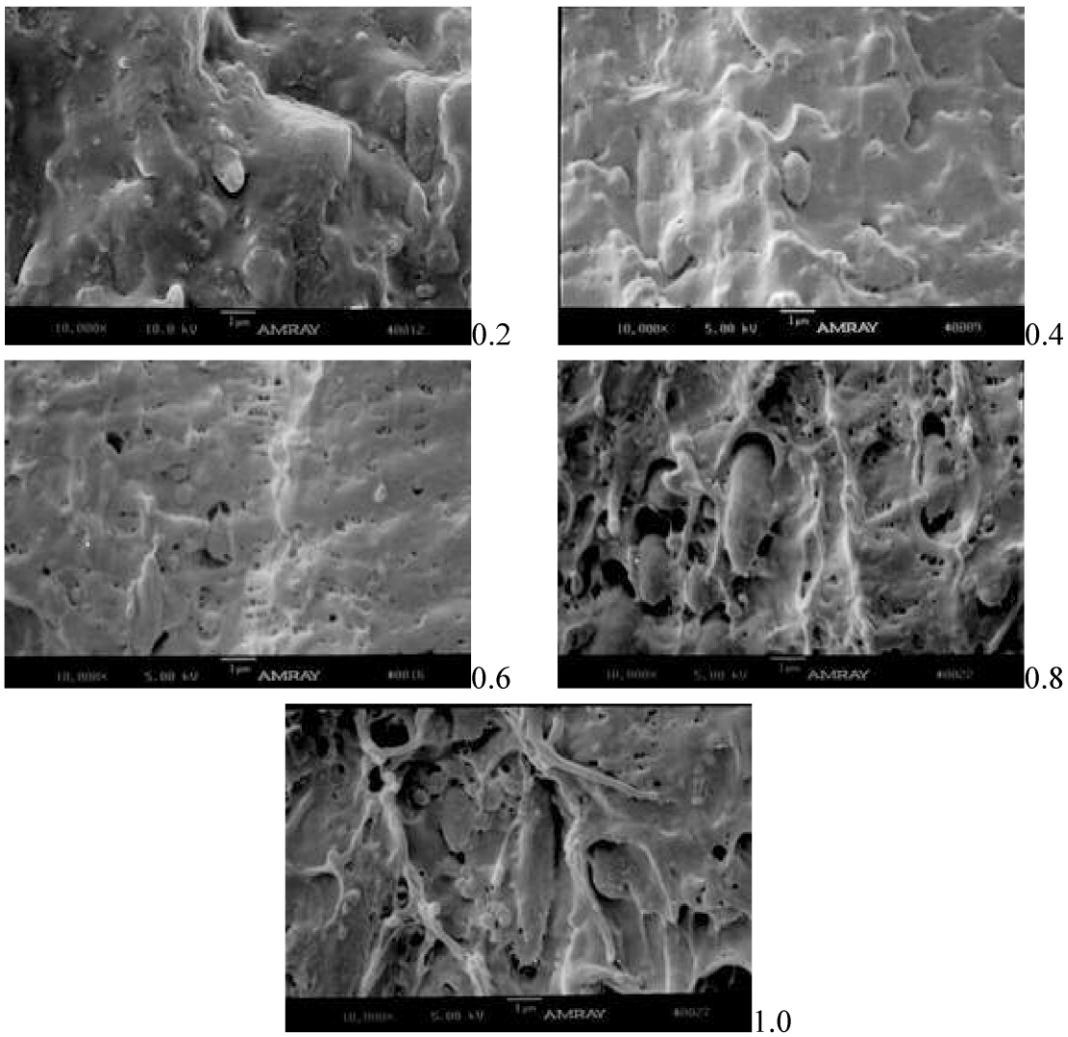

Fig. 14. Cryo-fractured surfaces of BD16 (figures on the micrograph indicating the level of applied true strain). Vertical loading.

Acknowledgements

This work is supported by the National Natural Science Foundation of China under grant of 10032010 and 10272005, by the Excellent Young Teachers Program of MOE, P.R. China, as well as by the PRA program between China and France. The authors would thank Mr J.-M. Hiver from School of Mines of Nancy, for the help to fulfill cyclic tension tests.

References

[1] Wong SC, Mai YW. Polymer 2000;41:5471–83.
[2] Wong SC, Mai YW. Polymer 1999;40:1553–66.
[3] Gonzales-Montiel A, Keskkula H, Paul DR. Polymer 1995;36(24): 4587–603.
[4] Gonzales-Montiel A, Keskkula H, Paul DR. Polymer 1995;36(24): 4605–20.
[5] Gonzales-Montiel A, Keskkula H, Paul DR. J Polym Sci B Polym Phys 1995;33:1751.
[6] Roeder J, DeOliveira RVB, Goncalves MC, Soldi V, Pires ATN. Polymer Test 2002;21:815–21.
[7] Darie RN, Brebu M, Vasile C, Kozlowski M. Polym Degrad Stab 2003;80(3):551–66.
[8] Zeng N, Bai SL, Cao K, G'Sell C, Mai YW. Polym Int 2002;51(12): 1439–47.
[9] Wang GT, Bai SL, Cao K, Hiver JM, G'Sell C. Polymer 2003;0. in press.
[10] G'Sell C, Aly-Helal NA, Jonas JJ. J Mater Sci 1983;18:1731.
[11] Bucknall CB, Clayton D, Keast WE. J Mater Sci 1972;7:1443.
[12] Gent AN, Park B. Mater Sci 1984;19:1947–56.
[13] G'Sell C, Hiver JM, Gehin F. Deformation, yield and fracture of polymers. London: The Institute of metals; 2000. p. 371–374.
[14] Bai SL, Chen JK, Huang ZP, Yu ZZ. J Mater Sci Lett 2000;19(17): 1587–9.
[15] Meddad A, Fisa B. J Appl Polym Sci 1997;64:653–65.
[16] Pukanszky B, Van Es M, Maurer FHJ, Voros D. J Mater Sci 1994;29: 2350–8.
[17] Meyer RW, Pruitt LA. Polymer 2001;42:5293–306.
[18] Bai SL, Liu ZD, Ju Y. Polym Int 2001;50:973–9.
[19] Drozdov AD, Christiansen JdeC. Euro Polym J 2003;39:21–31.
[20] G'Sell C, Hiver JM, Dahoun A. Int J Solids Struct 2002;39(13–14): 3857–72.